EEET ECOLOGICAL ENGINEERING & ENVIRONMENTAL TECHNOLOGY

Ecological Engineering & Environmental Technology 2024, 25(7), 46–62
https://doi.org/10.12912/27197050/187922
ISSN 2719-7050, License CC-BY 4.0

Received: 2024.04.15
Accepted: 2024.05.15
Published: 2024.06.01

Study on Wastewater Treatment in the Textile Industry by Adsorption of Reactive Red 141 Dye Using a Phosphogypsum/ Vanadium Composite Developed from Phosphate Industry Waste

Fatima Zahra Chajri[1,2], Meryem Bensemlali[1], Badreddine Hatimi[1], Asmae Sanad[1], Meryeme Joudi[1,2], Abdellatif Aarfane[1,3], Mustapha Siniti[4], Mina Bakasse[1], Abdoullatif Baraket [3], Hamid Nasrellah[1,3*]

[1] Faculty of Sciences, Laboratory of Organic Bioorganic Chemistry and Environment, Chouaib Doukkali University, 24000 El Jadida, Morocco

[2] Faculty of Sciences Ben M'Sik, Laboratory of Analytical and Molecular Chemistry, Hassan II University, BP 9167 Casablanca, Morocco

[3] Higher School of Education and Training, Chouaib Doukkali University, 24000 El Jadida, Morocco

[4] Faculty of Sciences, Laboratory of Coordination and Analytical Chemistry, Chouaib Doukkali University, 24000 El Jadida, Morocco

* Corresponding author's e-mail: nasrellah.h@ucd.ac.ma

ABSTRACT

A novel method has been explored based on the recovery of two industrial wastes V_2O_5 and phosphogypsum from the fertilizer production industry, which also provide a significant challenge due to their toxicity and environmental impact. To solve the problem of these two harmful wastes, these residues have been transformed into valuable resources, by the elaboration of Nanoparticles vanadate-hydroxyapatite (NPs-HAP/VAP) adsorbent, contributing a sustainable solution without requiring expensive or highly skilled work. This comprehensive investigation explores the adsorption of the reactive red 141 dye (RR 141) on $Ca_{10}(VO_4)_x(PO_4)_{6-x}(OH)_2$, with ($x_i$ = 0, 1.5, 3, 4.5, and 6). Using a Centered composite design (CCD), several parameters influencing the adsorption process were examined. The optimal adsorption capacity is 50 mg. g – 1 under optimal conditions 57.5 mg of the adsorbent dose, 152.5 mgL^{-1} for the RR 141, pH 8, 92.5 minutes of contact time, and incorporation ratio of 4.5 with an R^2 of 0.99. These results reinforce the effectiveness of our chosen CCD model. Kinetic analysis demonstrated a pseudo-order reaction model with an $R^2 > 0.92$, while the Sips isotherm describes the adsorption process. Thermodynamic studies revealed spontaneous adsorption, suggesting a physical character enhanced by a positive entropy variation.

Keywords: isotherm models, nanomaterial, kinetic analysis, valorization, thermodynamic studies.

INTRODUCTION

Water purification has become a global concern in recent decades because of declining water supplies and rising water pollution by industrialization and urbanization (Liang et al., 2019; Lin et al., 2022; Morin-Crini et al., 2022). Various industrial byproducts, including metals, lubricants, chemicals, dyes, and others, are examples of water pollutants (Ahmed et al., 2021; Ajiboye et al., 2021). Water contamination is mostly caused by dye leakage, which is mostly produced by the food, paper, textile, and printing sectors (Liu, 2020; Sharma et al., 2021; Singh et al., 2022).

Most commercial organic dyes fall under the group of azo dyes, which is why they are especially concerning (Bafana et al., 2011; Eltaboni et al., 2022; Hashemi and Kaykhaii, 2022). About 700,000 tons of azo dyes are produced annually worldwide. 70% globally are used, for instance, by the textile sector(Garg and Tripathi, 2017; Ibitoye et al., 2022). Regretfully, a

significant amount of these colors is not retained by textile fibers and, without proper treatment, end up in effluents, posing a substantial risk to aquatic life and the delicate balance of ecosystems. These azo dyes pose a cancer danger to living things since they are not only extremely poisonous but also non-biodegradable (Bafana et al., 2011; Chung, 2016; Hashemi and Kaykhaii, 2022; Ibitoye et al., 2022). It is essential to search for novel and financially feasible techniques to eliminate these azo dyes from textile wastewater due to their susceptibility to destruction by sunlight and aerobic digestion (Alabdraba and Bayati, 2014; Khan et al., 2013; Saratale et al., 2011).

Over the years, the development of textile wastewater treatment methods, including coagulation, membrane separation, anaerobic-aerobic treatment, photodegradation, electro-degradation, and adsorption, has drawn the attention of scientists over time (Holkar et al., 2016). Adsorption is one of these approaches that has shown to be very promising because of its ease of use, inexpensive operating costs, and capacity to effectively remove contaminants from contaminated water (Sophia and Lima, 2018). One of the major challenges in the field of adsorption is to develop adsorbents that combine high adsorption capacity and rapid reactivity while remaining economically affordable and environmentally friendly (Jebli et al., 2023; Jokić Govedarica et al., 2024; Srikaew et al., 2023). Although low-cost adsorbents have financial benefits, their adsorption capacity is often lower. To overcome these requirements, this studyfocused on the synthesis of nanoparticle vanadate-hydroxyapatite (NPs-HAP/VAP) adsorbents.

The dye RR141 is recognized for its presence in various industries, notably in the textile sector. However, It's well-known that its toxicity causes harm to the environment, aquatic organisms, and human health. Therefore, it is crucial to remove this dye from industrial wastewater to reduce its harmful impact. However, the current methods of detaching this pollutant can be a costly process, often requiring expensive adsorbents. To meet this challenge, our research effectively transformed industrial waste into nanocrystalline(Chajri et al., 2024). The production of phosphoric acid produced two wastes that were used to synthesize vanadate-apatite HAP/VAP: phosphogypsum and vanadium pentoxide waste. Well known for their toxicity, phosphogypsum (PG) was utilized as a source of calcium, while vanadium was obtained from V_2O_5 waste (Chajri et al., 2024). The proposed adsorbent was synthesized by using a straightforward process that involved combining sodium hydroxide, phosphoric acid, and vanadium pentoxide with different amounts of hydrated anhydrous gypsum, without adjusting the pH. The reaction was allowed to run for 48 hours at room temperature. The process produces both phosphate and vanadate apatite with high yields by experimenting with different ratios of starting chemicals. Furthermore, we varied the vanadium ratios in the synthesis to explore different vanadate-apatite compositions and optimize conditions to develop a material suited for the adsorption of the Reactive-Red – 141 dye (RR141) (Chajri et al., 2024). The nanoscale hydroxyapatite $Ca_{10}(PO_4)_6(OH)_2$ has great potential as an adsorbent due to its specific structure, conferring ion exchange properties and high adsorption affinity exchange properties and high adsorption affinity for many pollutants(Ibrahim et al., 2020; Pai et al., 2021).

Thus, our study is part of an effort to optimize the adsorption efficiency of the RR141 dye on vanadate/hydroxyapatite using advanced experimental approaches, paving the way for more effective solutions for textile wastewater treatment. To this end, we have taken a Design of experiments (DOE) approach, in association with the response surface methodology (RSM) (Bezerra et al., 2008; Bouchelkia et al., 2023), which enables us to identify possible interactions and correlations between these crucial variables, to obtain the optimal conditions for the removal process. Specifically, we studied the adsorption of the RR141 dye onto vanadate/hydroxyapatite, examining key factors such as dye concentration, pH, adsorbent mass, time, and different ratios of vanadate incorporated into the apatite. To analyze these factors in depth, we used the centered composite design (CCD) to enhance the nano-Hap-VAP as an effective adsorbent for azo dye removal RR141. In addition, to measure the correlation between dye concentration and adsorbed quantity, our experiments also involved an in-depth examination of adsorption isotherms and an assessment of the thermodynamics of the adsorption process. These results allow us to have a deep understanding of the adsorption behavior and pave the way for more precise optimization of the process.

MATERIALS AND METHODS

Materials

The dye utilised in this work is Reactive Red 141, which is a commercial product, purchased from BASF Germany. It is an azo molecule with a very high molecular weight of 1774.2 g·mol^{-1} and the formula $C_{52}H_{26}Cl_2N_{14}Na_8O_{26}S_8$. Table 1 and Figure 1 show the properties and molecular structure of Reactive Red 141.

Experimental methodology

The range of vanadate compounds incorporated into the calcium hydroxyapatite structure $(VO_4)^{3-}$/HAP nanomaterial $(Ca_{10}(VO_4)_X(PO_4)_{6-X}(OH)_2$ with (x = 0, 1.5, 3, 4.5, and 6) was synthesized from phosphogypsum waste as a source of calcium, and vanadium pentoxide as a source of vanadate in this novel study where they are generated from the manufacturing sulfuric acid. This innovative strategy is based on the prudent use of accessible materials and industrial waste, contributing to resource sustainability while opening new opportunities for the applications of the produced materials. This work includes detailed descriptions of the synthesis methods and characterizations used (Chajri et al., 2024). The findings of this study provide intriguing potential for resource management while reacting to present environmental and technical problems. The nanoparticles $(VO_4)^{3-}$incorporated calcium HAP were synthesized at ambient temperature in an aqueous solution by dissolving various quantities of $CaSO_4$, V_2O_5, H_3PO_4, and

Table 1. Properties of reactive red 141(RR-141)

Parameter	Value
Functional group	Azo dye
Color index name	Reactive Red 141(RR141)
Molecular mass (g·mol^{-1})	1774.2
Molecular formula	$C_{52}H_{26}Cl_2N_{14}Na_8O_{26}S_8$
Wavelength absorbed (nm)	545
Solubility (g·L^{-1})	150
Composition	Diazo (-N = N – bond)

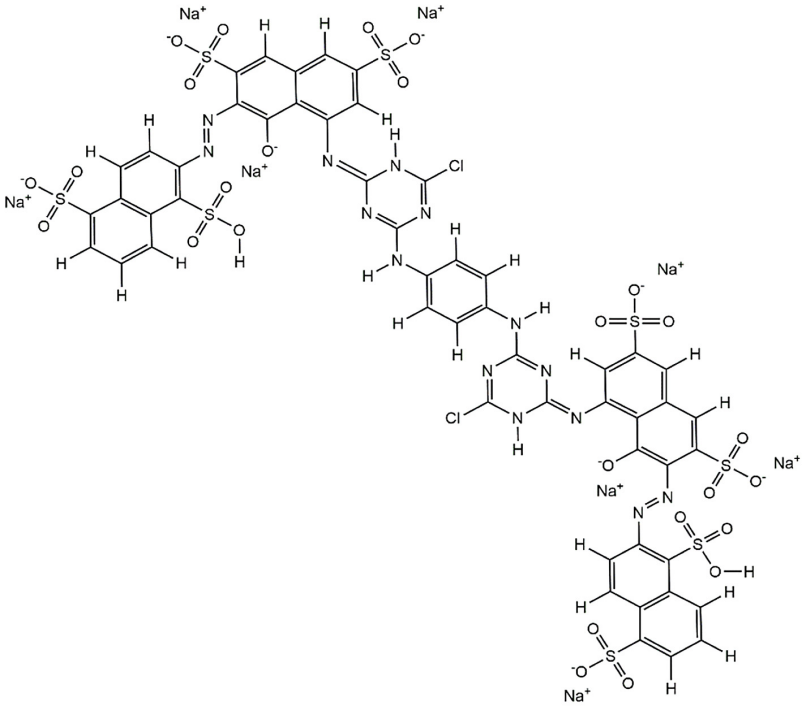

Figure 1. Chemical structure of the azo dye reactive red (RR-141)

NaOH in 100 mL, the mixture was agitated for 48 hours at room temperature using a mechanical shaker. The produced NAPs-VAP/HAP was then filtered out of the solution, and the resulting powder was washed multiple times with water until a clear and neutral supernatant was obtained. In the end, the solid samples were dried at 105 °C for 24 hours before being calcined at 900 °C for 3 hours.

To prepare the synthetic wastewater, the RR-141 dye was dissolved in distilled water to make a stock solution of 1g·L^{-1}. Each flask was filled with 50 ml of the printing ink wastewater and was continuously mixed based on the following crucial parameter range presented in Table 2. Specific amount of the sample $Ca_{10}(VO_4)_X(PO_4)_{6-X}(OH)_2$ with (x = 0, 1.5, 3, 4.5, and 6) was added to 50 mL of RR-141 dye solution of varying concentrations (10 to 200 mg·L^{-1}). The mixture was stirred with a magnetic agitator to determine the equilibrium time at 293 K. After stirring, 4 mL of the suspension was taken out and separated by centrifugation at 4600 rpm for 15 min using a BIOBASE BK-H2018J centrifuge. The determination of dye residual concentration was done spectrophotometrically on a JASCO V-630 UV Visible spectrometer by measuring absorbance at a maximum wavelength λ_{max} of 545 nm.

To investigate the effect of pH on adsorption, a series of dye solutions were generated by varying the pH from (2-10) with dilute HCl (0,1N) or NaOH (0,1N) solutions. Other factors tested were adsorbent dosage (10 to 200 mg·L^{-1}), starting dye RR-141 concentration (10 to 200 mg·L^{-1}), and stirring time (10 to 120 min). Table 2 depicts the various ranges and value conditions of the main RR-141 adsorption property factors.

The removal percentage of RR-141 and the adsorption capacity values at equilibrium at any given time t and equilibrium were determined by Equations 1 and 2 respectively.

$$\% \text{ dye removal} = ((C_0 - C_e)/C_0)\cdot 100 \quad (1)$$

$$q_e \text{ (mg.g}^{-1}) = ((C_0 - C_e)\cdot(V/W)) \quad (2)$$

where: C_0 (mg·l^{-1}) – the initial RR-141 dye concentration, C_e – the RR-141 dye concentration at equilibrium, V – the volume of the solution, W(g) is the amount of the adsorbent in the solution.

As part of the study of reaction kinetics, first-order and pseudo-second order (PFO, PSO) respectively, were used to explore the adsorption mechanism of RR-141 on the synthesized adsorbent $Ca_{10}(PO_4)_{1.5}(VO_4)_{4.5}(OH)_2$ at intervals of 5, 15, 25, 35, 45, 55 and 65 minutes. To assess adsorption capacity, we used Langmuir, Freundlich, and Sips isotherm methods. By fitting a suitable adsorption isotherm model to the experimental data, the relationship between the adsorbed quantity and the quantity remaining in the solution at equilibrium during the adsorption process was studied, and characteristic parameters for each isotherm were determined. Using nonlinear regression curves, different equations of isotherm models (Table 3) were considered to predict the behaviors of RR141 dye concerning the adsorbent. In the present study, factors such as contact time of 65 min, pH = 8, the adsorbent dosage of 57.5 mg, and the ratio of the adsorbent $Ca_{10}(PO_4)_{1.5}(VO_4)_{4.5}(OH)_2$, providing maximum removal of RR141, were kept constant for each adsorption isotherm experiment. Additionally, the temperature was varied from 20 to 50 °C to evaluate its effect on the adsorption phenomenon and deduce thermodynamic parameters. It is important to note that all adsorption data presented in this article are the average of three separate experiments.

DESIGN OF EXPERIMENTS

Point of zero charge

The experiments were conducted using a batch method. First, 0.25 g of $Ca_{10}(VO_4)_{4.5}(PO_4)_{1.5}(OH)_2$

Table 2. The experimental design conditions for RR-141 adsorption process

Factors	Unit	Coded variables	-α	-1	0	+1	+α
Ratios of the adsorbent	-	X_1	0	1.5	3	4.5	6
Dye concentration	mg/l	X_2	10	57.5	105	152.5	200
Adsorbent dose	mg	X_3	10	57.5	105	152.5	200
pH	-	X_4	2	4	6	8	10
Time	min	X_5	10	37.5	65	92.5	120

Table 3. The kinetic model, isotherm, and thermodynamic equations

Models	Non-linear equation	Parameter	Plot	Ref
Isotherm model				
Langmuir	$q_e = \frac{q_m K_l C_e}{1 + K_l C_e}$	q_m, K_l	q_e vs C_e	[26], [27]
Freundlich	$q_e = K_F C_e^{1/n}$	K_F, n	q_e vs C_e	[28], [29]
Sips	$q_e = \frac{q_s a_s C_e^{1/ns}}{1 + a_s C_e^{1/ns}}$	q_s, a_s, n_s	q_e vs C_e	[30], [31]
Kinetic model				
Pseudo first order (PFO)	$q_t = (q_e - exp^{-K_L t})$	K_L, q_e	q_t vs t	[32], [33]
Pseudo second order (PSO)	$q_t = \frac{K_2 q_e^2 t}{1 + K_2 q_e t}$	K_2, q_e	q_t vs t	[34]

was added to different closed conical flasks 50 mL containing a potassium nitrate (KNO_3) solution that was 0.1 M in volume and had adjusted to various pH levels (2, 4, 6, 7, 8, 10). NaOH (0,1 N) and HCl (0,1 N) were used to modify the initial pH solution (pH_i). A magnetic stirrer was used to mix the prepared solution for 24 hours at 25 °C while operating at 2.5 Hz. The final pH solution (pH_f) of the supernatant was determined.

Experimental range delimitation

The experimental ranges for the five selected parameters were determined based on preliminary laboratory testing to optimize the purification process, as shown in Table 2. Each of these factors was assessed at three different coded levels: (-1) for low, (0) for mid, and (+1) for high. Table 2 summarizes the components used and their experimental ranges. The coded variables, labelled X_i (where i = 1, 2, 3, 4, 5), were determined using Equation 3:

$$X_i = {(x_i \pm x_0)}/{\Delta x_i} \quad (3)$$

where: x_i – representing real values and x_0 representing variation increments. The experimental ranges for X_1 are 0–6, 10–200 mg. L^{-1} for X_2, and 10–200 mg. L^{-1} for X_3, 2–10 for X_4, and 10–120 min for X_5.

Mathematical model and experimental matrix description

The CCD model was used to optimize the removal of RR-141 by $Ca_{10}(VO_4)_X(PO_4)_{6-X}(OH)_2$ (with x = 0, 1.5, 3, 4.5, and 6) nanoparticles. This model is represented in quadratic form, to fit the response variables, a second-order mathematical model in the form of a quadratic polynomial equation was used by the following Equation 4:

$$Y_i = \beta_0 + \sum(\beta_i X_i) + \sum(\beta_{ii} X_i^2) + \sum(\beta_{ij} X_i X_j) + \varepsilon \quad (4)$$

Y_i denotes the response variable to be modeled in this equation, whereas X_i and X_j denote the independent parameters that influence Y. The terms β_0, β_i, β_{ii}, and β_{ij} denote the constant term, initial linear coefficient, quadratic coefficient, and interaction coefficient, respectively. Table 4 shows an experimental matrix based on Hadamard's principle, with 36 experiments based on the CCD particular combinations. As dependent variables, the experimental outcomes of adsorption capacity RR-141 by $Ca_{10}(VO_4)_X(PO_4)_{6-X}(OH)_2$ with x = 0, 1.5, 3, 4.5, and 6) nanoparticles.

Design of experiments and data analysis

JMP PRO v16.0 (SAS) (JMP 2023; Jones and Sall 2011) and Stat Soft STATISTICA 12 (Hilbe 2007; Statsoft 2013) were used for the experimental design and statistical analysis of data. CCD associated to response surface methods were employed to optimize five essential parameters: ratio of the adsorbent, dye concentration, adsorbent dose, pH, and time. The Fisher's test and the p-value of 0.05 for ANOVA (Driouich et al., 2020) were used for statistical analysis, and the coefficient of determination R^2 validated the model by comparing computed values with predictions (R^2 = 0.995) as shown in Figure 2. The CCD is a second-order response surface model that includes extreme values and has three-point types: cubic, axial, and central. Considering the five variables, the total number of trials is N = 10 factorial experiments + 16 axial experiments + 10 central experiments.

Table 4. Calculation of experimental data using a central composite design for the adsorption capacity qe ($mg \cdot g^{-1}$)

Logical order	Ratio of the adsorbent $Ca_{10}(VO_4)_x(PO_4)_{(6-x)}(OH)_2$		RR141 dose (mg/l)		Adsorbent dose (mg)		pH	Time (min)		Adsorption capacity q_e($mg \cdot g^{-1}$) (Y_2)		
	X_1	x_1	X_2	x_2	X_3	x_3	X_4	x_4	X_5	x_5	Experimental	Predicted
1	0	3	0	105	0	105	0	6	-2	10	9.32	11.39
2	-1	1.5	-1	57.5	-1	57.5	-1	4	-1	37.5	16.29	15.83
3	1	4.5	1	152.5	-1	57.5	-1	4	-1	37.5	8.69	7.81
4	1	4.5	-1	57.5	1	152.5	-1	4	-1	37.5	13.75	13.26
5	-1	1.5	1	152.5	1	152.5	-1	4	-1	37.5	4.87	4.56
6	1	4.5	-1	57.5	-1	57.5	1	8	-1	37.5	33.03	31.89
7	-1	1.5	1	152.5	-1	57.5	1	8	-1	37.5	18.05	17.09
8	-1	1.5	-1	57.5	1	152.5	1	8	-1	37.5	4.15	3.58
9	1	4.5	1	152.5	1	152.5	1	8	-1	37.5	31.15	30.15
10	0	3	0	105	0	105	-2	2	0	65	2.99	3.07
11	0	3	0	105	-2	10	0	6	0	65	21.91	23.27
12	0	3	-2	10	0	105	0	6	0	65	7.34	7.93
13	-2	0	0	105	0	105	0	6	0	65	3.56	3.79
14	0	3	0	105	0	105	0	6	0	65	0.46	0.82
15	0	3	0	105	0	105	0	6	0	65	1.76	0.82
16	0	3	0	105	0	105	0	6	0	65	0.37	0.82
17	0	3	0	105	0	105	0	6	0	65	1.57	0.82
18	0	3	0	105	0	105	0	6	0	65	0.59	0.82
19	0	3	0	105	0	105	0	6	0	65	0.98	0.82
20	0	3	0	105	0	105	0	6	0	65	1.01	0.82
21	0	3	0	105	0	105	0	6	0	65	1.18	0.82
22	0	3	0	105	0	105	0	6	0	65	0.69	0.82
23	0	3	0	105	0	105	0	6	0	65	1.22	0.82
24	2	6	0	105	0	105	0	6	0	65	17.5	18.94
25	0	3	2	200	0	105	0	6	0	65	17.65	18.73
26	0	3	0	105	2	200	0	6	0	65	4.44	4.74
27	0	3	0	105	0	105	2	10	0	65	16.05	17.65
28	1	4.5	-1	57.5	-1	57.5	-1	4	1	92.5	2.54	2.4
29	-1	1.5	1	152.5	-1	57.5	-1	4	1	92.5	20.15	20.19
30	-1	1.5	-1	57.5	1	152.5	-1	4	1	92.5	14.73	15.15
31	1	4.5	1	152.5	1	152.5	-1	4	1	92.5	6	6.01
32	-1	1.5	-1	57.5	-1	57.5	1	8	1	92.5	7.08	6.86
33	1	4.5	1	152.5	-1	57.5	1	8	1	92.5	50.01	49.36
34	1	4.5	-1	57.5	1	152.5	1	8	1	92.5	4.06	3.8
35	-1	1.5	1	152.5	1	152.5	1	8	1	92.5	0.88	0.8
36	0	3	0	105	0	105	0	6	2	120	6.9	6.5

Note: X_i – coded factor; x_i – real factor; Y_i – responses.

RESULT AND DISCUSSION

Regression variance analysis ANOVA

Table 5 presents the results of the variance analysis (ANOVA) applied to the quadratic model for the RR141 adsorbance capacity, employing different materials of $Ca_{10}(VO_4)_X(PO_4)_{6-X}(OH)_2$ with the variation of the incorporation ratio of the (VO_4^{3-}) by (PO_4^{3-}) with (x = 0, 1.5, 3, 4.5, and 6) nanoparticles. The quadratic model studied is depicted in Table 5, based on ANOVA

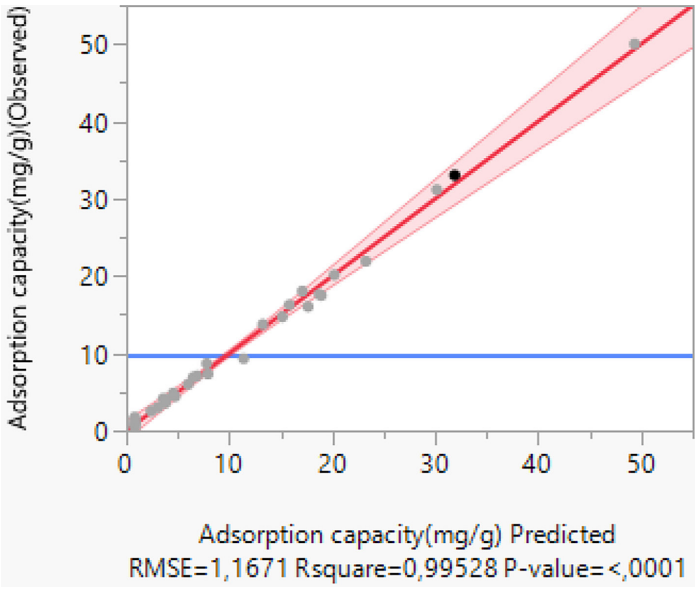

Figure 2. The plot of the relationship between the predicted and actual values for adsorption capacity (mg/g) of dye RR-141

with a 95% confidence level, and according to the F-test, the result shows that the regression value ($p = 0.001$) is below than the 0.05 criterion. Furthermore, the experimental Fisher-Snedecor factor (experimental F = 158.1347) is highly exceeding the tabulated critical value (critical F = 5.25 for $F_{0.001}$ (20, 15)) (Esbensen et al., 2002). These results demonstrate that the experimental value of F is significantly higher than expected, validating the significance of the CCF model (R^2 is near to 100%, indicating that the response models better match the real data Figure 2) (Willmott 1981).

Table 5. Regression variance analysis (ANOVA) for adsorption capacity q_e (mg/g)

Source of variation	Degree of freedom	Sum of squares	Mean square	F_{exp}	P-Value	Significance
Model	20	4307.7917	215.390	158.1347	<0.0001	***
Residual	15	20.4310	1.362			
Total	35	4328.2227				

Note: significant at a level of 0.1% ($F_{0.001}$ (20, 15) = 5.25) (Esbensen et al., 2002).

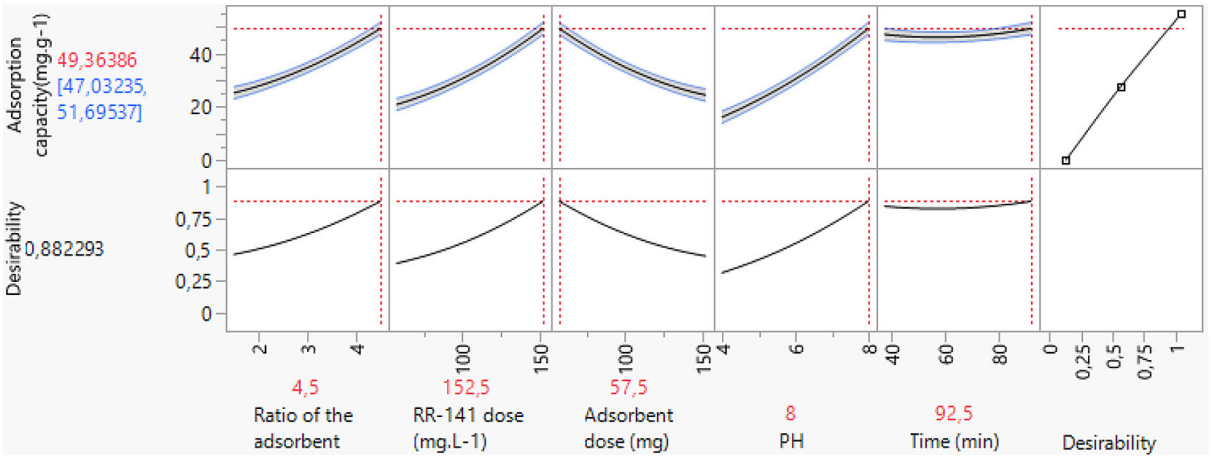

Figure 3. Main effects of parameters on the adsorption capacity ($mg \cdot g^{-1}$)

Graphical analysis of factor effects

Effect of pH

The effect of pH on the adsorption of RR141 was investigated in Figure 3. It is noted that the pH affects the capacity for pollutant adsorption as well as the adsorption rate. We also noticed that a progressive increase in the adsorption rate from pH 4 to pH 8, with an adsorption capacity of 49.36 mg/g at pH = 8. According to this pattern, slightly basic circumstances increase effective contaminant adsorptions. As shown in Figure 4 (pH point of zero charge indicates the impact of pH on zeta potential), which leads to enhanced efficiency at higher pH levels. This behaviour is in line with the zero-charge point, where the adsorbent surface is primarily positive at a pH below 8.73 and adsorbs negative dye molecules (Hafdi et al., 2020a; Kosmulski, 2014; Sansenya et al., 2022).

Effect of adsorbent dose

The dose of adsorbent also has a significant effect on responses. With increasing doses of the adsorbent ($Ca_{10}(VO_4)_X(PO_4)_{6-X}(OH)_2$ with x = 0, 1.5, 3, 4.5, and 6) from 57.5 to 152.5 mg/L, the capacity of adsorption starts to decrease from 47.13 to 30.15 mg/g. This implies that using the right quantity of adsorbent is crucial to maximizing adsorption effectiveness. The efficiency can be decreased by the agglomerated particles dispersing when there is too much adsorbent present (Bonyadi et al., 2022).

Effect of dye dose

The dye dose has a significant impact on the responses. the highest 47.13 mg/g and lowest 31.88 mg/g adsorption capacities were obtained at concentrations of 152.5 mg/L and 57.5 mg/L, respectively. This suggests that an appropriate dose of dye is required to maximize adsorption. On the other hand, a high RR-141 dye 152.5 mg/L, can match with fewer quantities of the adsorbent 57.5 mg/L as shown in Figure 3 (optimal conditions).

Effect of ratio of the adsorbent

The adsorbent ratio, which has been identified as a crucial component, has a considerable impact on the observed results. By changing the adsorbent ratio of $Ca_{10}(VO_4)_X(PO_4)_{6-X}(OH)_2$ from x = 1.5 to x = 4.5, a clear trend emerges. adsorption capacity evolves significantly. Initially, at a ratio of x = 1.5, the adsorption capacity is recorded at 27 mg/g, while an increase in the adsorbent ratio at x = 4.5 propels it to 49.36 mg/g. This significant variation in adsorption capacity as a function of the adsorbent ratio plays a key role in improving the efficiency of the adsorption process.

Time effect

As shown in Figure 3 the duration of the experiment had a significant impact on the response of RR-141 adsorption capacity. For instance, when the duration was increased from 37.5 min to 92.5 min, the adsorption capacities rose from 47.13 mg/g to 49.36 mg/g (with a p-value < 0.05 indicating statistical significance). These results imply that dye removal was faster initially due to the availability of many active surface sites for dye adsorption. However, as time progressed, the removal process stabilized due to saturation of the adsorption sites.

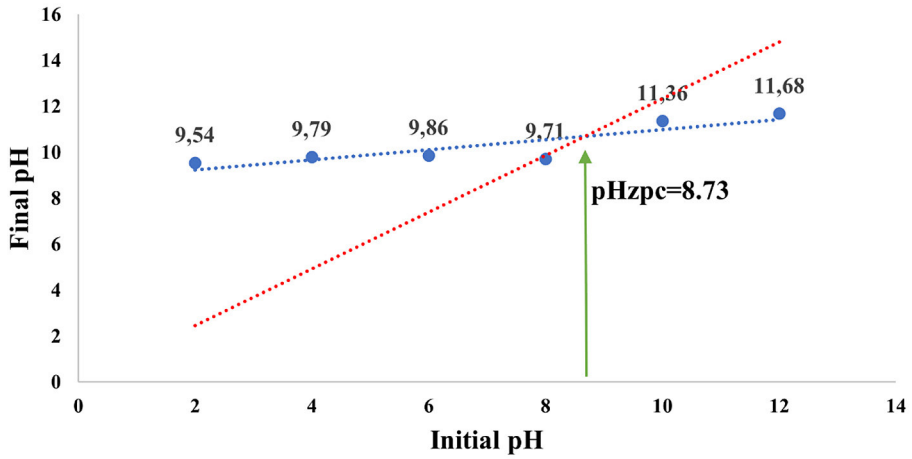

Figure 4. The impact of pH on the zeta potential of the $Ca_{10}(VO_4)_{4.5}(PO_4)_{1.5}(OH)_2$

Optimum operational conditions

In this study, the results were analyzed using the CCD to obtain the highest dye removal rate. According to the quadratic model, the highest adsorption capacity (50.01 $mg \cdot g^{-1}$) was found at the pH of 8, an adsorbent dose of 57.5 $mg \cdot L^{-1}$, contact time of 92.5 min, the ratio of the adsorbent was found to be $Ca_{10}(VO_4)_{4.5}(PO_4)_{1.5}(OH)_2$, and the RR-141 dose of 152.5 $mg \cdot L^{-1}$.

Statistical analysis of factors effects

The estimated regression coefficients, F – value, and P – values for all the linear, quadratic, and interaction effects of the parameters are given in Table 6. As observed, the linear effect of X_1, X_2, X_3, X_4, X_5, the interaction effects $X_1 \cdot X_2$, $X_2 \cdot X_3$, $X_1 \cdot X_4$, $X_2 \cdot X_4$, $X_3 \cdot X_4$, $X_1 \cdot X_5$, $X_2 \cdot X_5$, $X_3 \cdot X_5$, $X_4 \cdot X_5$ and quadratic effect X_1^2, X_2^2, X_3^2, X_4^2, X_5^2 are significant model terms (P-value < 0.01). As a result, $X_1 \cdot X_4 > X_3$ (57,5; 152,5) > $X_3 \cdot X_3 > X_1 > X_4$ (4; 8) > $X_2 \cdot X_2$ define the most significant model term influence of the adsorption capacity of RR-141, with F-value equal to 587.4252, 378.2426, 255.3661, 252.8391, 234.1624 and 229.8403 respectively. This study validates the efficiency of RR-141 removal as a function of those different factors. Similar observations were reported by (Hafdi et al., 2020b), which supported the present finding.

Pareto diagram analysis

By using The Pareto chart, we can prioritize the importance of factors in our RR-141 elimination experiment. The results of our model revealed that twelve terms have a significant influence on the adsorption capacity of RR-141 (explaining more than 80% of the total effects). As illustrated in Figure 5 we can observe from the statistics that some factors have a bigger influence than others. The adsorption capacity of RR-141 is most positively impacted by the component X_3^2 (the quadratic effect of adsorbent dose), the combinations $X_2 \cdot X_3$ (RR141 dose·adsorbent dose), $X_1 \cdot X_4$ (ratio of the adsorbent·pH), and $X_4 \cdot X_5$ (pH·time) and X_1^2 (the quadratic effect of the adsorbent ratio) among these parameters.

In fact, we find a considerable increase in the percentage of contaminant elimination. when these components are present at certain levels. However, the important effects of the component X_4^2 (the square of pH), the interaction $X_1 \cdot X_5$ (ratio of the adsorbent·time) are marginally less pronounced. Importantly, these elements are essential to comprehending and improving our adsorption process. Using these findings, we can specifically target these factors while optimizing our system to maximize the adsorption capacity of RR-141. The significance of these terms is also confirmed by their corresponding P-values, which were less than 0.05, as illustrated in Table 6.

Validation of the model

In this study, we analyzed the relationship between the experimental and predicted values of adsorption capacity using the design-of-experiments method, as presented in Tables 7 and 8. It is noted that, experimental values for adsorption capacity ranged from around 0.37 to 50, while the values predicted by our model ranged from 0.81 to 49.36. The residuals, indicating the difference between predicted and experimental values, show a significant dispersion, ranging from -2.07 to 1.14 for adsorption capacity. The most residuals are close to zero, indicating reasonable agreement between predicted and experimental values in many cases. However, high residuals, particularly those above 2, suggest significant divergence in some cases, these data more closely and potentially improve our model for more accurate predictions. Similarly, Figure 2 is fully consistent with our previous interpretations. In fact, the high coefficient of determination $R^2 = 0.993$ for adsorption capacity, indicates an extremely strong correlation between the predicted values and experimental observations. This high coefficient of determination confirms the validity and robustness of the defined model in predicting q_e ($mg \cdot g^{-1}$) adsorption capacity. It is consistent with the previous interpretations, and the experimental data highlights the validity of our model in many situations. Table 7 summarizes the definition of appropriate locations for the best adsorption capacity ($mg \cdot g^{-1}$) for the dye RR141.

Two-dimensional iso-response plots and three-dimensional response surfaces were generated using STATISTICA software to assess the relative impact of two factors while keeping the others constant (Driouich et al., 2020). These representations, which are based on the regression equation and generated from the quadratic model's equations, seek to comprehend the influences

Table 6. Estimated regression coefficients and corresponding F and P values for RR141 adsorption capacity q_e ($mg \cdot g^{-1}$)

Source of variation	Estimated coefficient	Erreur standard	Sum of squares	$F_{experimental}$	P-value	Significances
Constant	0.8180947	0.3639				
x_1 (1.5; 4.5)	3.7880458	0.238228	344.38299	252.8391	<.0001*	***
x_2 (57.5; 152.5)	2.7006708	0.238228	175.04695	128.5160	<.0001*	***
x_3 (57.5; 152.5)	-4.633171	0.238228	515.19053	378.2426	<.0001*	***
x_4 (4; 8)	3.6454542	0.238228	318.94407	234.1624	<.0001*	***
x_5(37.5; 92.5)	-1.223771	0.238228	35.94276	26.3885	0.0001*	***
x_1*x_2	2.5475313	0.291769	103.83865	76.2363	<.0001*	***
x_1*x_3	-0.147394	0.291769	0.3476	0.2552	0.6208	NS
x_2*x_3	-1.983131	0.291769	62.92495	46.1982	<.0001*	***
x_1*x_4	7.0715563	0.291769	800.11052	587.4252	<.0001*	***
x_2*x_4	3.7102938	0.291769	220.26048	161.7108	<.0001*	***
x_3*x_4	-3.726106	0.291769	222.14188	163.0921	<.0001*	***
x_1*x_5	-1.467806	0.291769	34.47128	25.3081	0.0001*	***
x_2*x_5	3.3180563	0.291769	176.15196	129.3272	<.0001*	***
x_3*x_5	-1.999069	0.291769	63.94041	46.9438	<.0001*	***
x_4*x_5	-1.511694	0.291769	36.56349	26.8442	0.0001*	***
x_1*x_1	2.6370592	0.206312	222.53059	163.3775	<.0001*	***
x_2*x_2	3.1277842	0.206312	313.05708	229.8403	<.0001*	***
x_3*x_3	3.2968967	0.206312	347.82488	255.3661	<.0001*	***
x_4*x_4	2.3846592	0.206312	181.97118	133.5996	<.0001*	***
x_5*x_5	2.0321592	0.206312	132.14947	97.0215	<.0001*	***

Note: non-significant; ***: significant at a level of 0.1% ($F_{0.001}(1, 15) = 16.59$); **: significant at a level of 1% ($F_{0.010}(1, 15) = 8.68$); *: significant at a level of 5% ($F_{0.050}(1, 15) = 4.54$) (Esbensen et al., 2002); $Y(q_e(mg/g)) = 0.8180947+3.6905417X_1+2.7006708X_2-4.633171X_3+3.6454542X_4-1.223771X_5+2.5475313X_1 \cdot X_2-1.983131X_2 \cdot X_3+7.0715563X_1 \cdot X_4+3.7102938X_2 \cdot X_4-3.726106X_3 \cdot X_4-1.467806X_1 \cdot X_5+3.3180563X_2 \cdot X_5-1.999069X_3 \cdot X_5-1.511694X_4 \cdot X_5+2.6370592X_1^2+3.1277842X_2^2+3.2968967X_3^2+2.3846592X_4^2+2.0321592X_5^2$; with ($\beta_0 = 0.8180947$) being a constant that is independent of any factor.

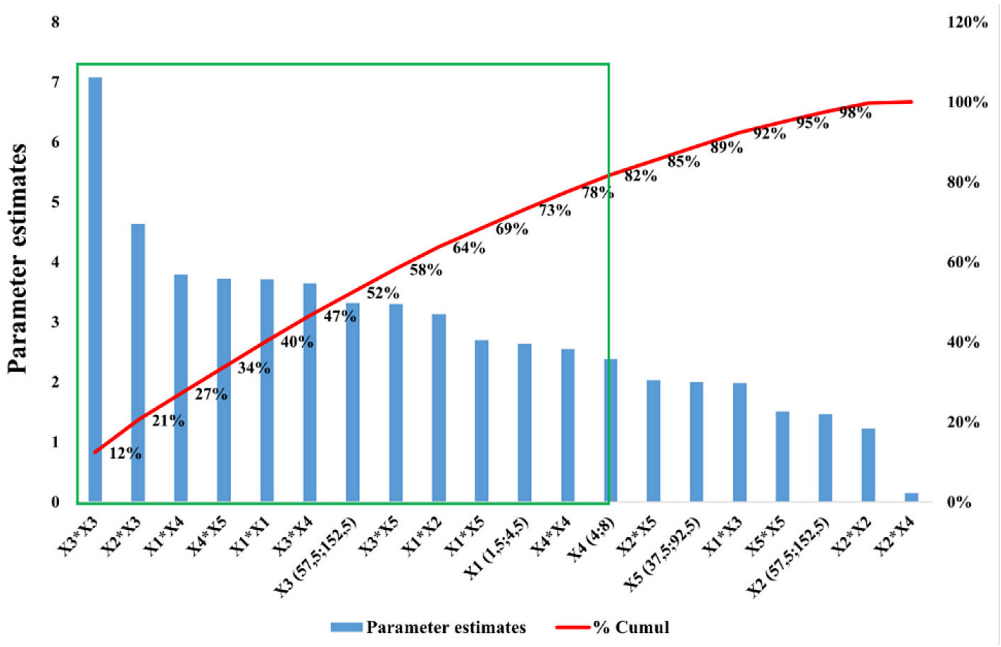

Figure 5. Pareto diagram for the RR141 adsorption capacity of analysis

Table 7. The scale of the desirability of the RR141 adsorption capacity

Value	Adsorption capacity (mg·g^{-1})	Desirability
Hight value	55	0.9819
Mean value	27.5	0.5
Low value	0	0.066

of factors on response and identify optimal conditions for the responses under study.

Response surfaces and iso-response curves illustrate the correlation between the independent factors (pH, adsorbent ratio, dye RR141 concentration, and adsorbent dose) and the dependent response (the adsorption capacity). These curves

Table 8. Experimental RR-141 adsorption capacity q_e (mg·g^{-1}) with experimental, predicted and residual values

Adsorption capacity q_e (mg·g^{-1})			
Logical order	Experimental	Predicted	Residual
1	9.3218	11.39427	-2.07247
2	16.2875	15.83166	0.45584
3	8.6869	7.80594	0.88096
4	13.7506	13.25546	0.49514
5	4.8716	4.56004	0.31156
6	33.0309	31.88901	1.14189
7	18.0498	17.09149	0.95831
8	4.1476	3.5751	0.5725
9	31.1523	30.15469	0.99761
10	2.9948	3.06582	-0.07102
11	21.9075	23.27202	-1.36452
12	7.335	7.92789	-0.59289
13	3.5645	3.79024	-0.22574
14	0.4597	0.81809	-0.35839
15	1.7644	0.81809	0.94631
16	0.3743	0.81809	-0.44379
17	1.569	0.81809	0.75091
18	0.5948	0.81809	-0.22329
19	0.9832	0.81809	0.16511
20	1.01467	0.81809	0.19658
21	1.1808	0.81809	0.36271
22	0.6921	0.81809	-0.12599
23	1.21684	0.81809	0.39875
24	17.4993	18.94242	-1.44312
25	17.6546	18.73057	-1.07597
26	4.435	4.73934	-0.30434
27	16.0498	17.64764	-1.59784
28	2.5434	2.40224	0.14116
29	20.1508	20.19321	-0.04241
30	14.7257	15.15393	-0.42823
31	6.004	6.00711	-0.00311
32	7.0797	6.86118	0.21852
33	50.0075	49.36386	0.64364
34	4.0571	3.79928	0.25782
35	0.8765	0.80225	0.07425
36	6.9028	6.49919	0.40361

for adsorption capacity are displayed in Figure 6a along with the interaction impact between pH and adsorbent dose at fixed time points of 92.5 minutes, 4.5 adsorbent ratio, and 152.5 mgL^{-1} dye concentration (RR141). The findings indicate that when the adsorbent dose is decreased, the adsorption capacity significantly increases. Additionally, when the adsorbent dose is between 5 $mg \cdot L^{-1}$ and 60 mg, and the pH is between 8 and 11, the optimal zone for maximal adsorption capacity is attained.

Figure 6b shows that, with a 152.5 mgL^{-1} RR141 concentration, 57.5 mg of adsorbent, and 92.5 minutes of contact time, the adsorption capacity increases as the pH rises. According to these results, with little fluctuation in these responses when the adsorbent ratio varies. Consequently, Figure 6c shows that an increase in concentration corresponds to an increase in adsorption capacity, which explains the results observed. In summary, these findings indicate that the higher concentration of RR141 is due to the higher surface area of the adsorbed dose present in the solution, which in turn creates a stronger driving force to accelerate the migration of RR141 dye molecules to the active adsorbent (binding) sites of $Ca_{10}(PO_4)_{1.}5(VO_4)_{4.5}(OH)_2$. The study has revealed the remarkable efficacy of the adsorbent material developed from waste materials in removing the dye RR141 from wastewater. In comparison to other frequently utilized adsorbent materials such as activated carbons, Nickel oxide doped natural phosphate (NP/NiO) or chitosan and zeolitic imidazolate framework – 8 (ZIF-8), the $Ca_{10}(VO_4)_x(PO_4)_{6-x}(OH)_2$ showed a significant adsorption capacity. Table 9 shows a comparison of waste-based adsorbents and their adsorption, highlighting the superior performance of this study.

Kinetic study

The pseudo-first order (PFO) and pseudo-second order (PSO) kinetic models' relative R^2 values are displayed in Table 10. The results reveal that R^2 values for the PFO are below 0.8, while those for the PSO are predominantly above 0.92, even reaching close to 0.99. These results indicate

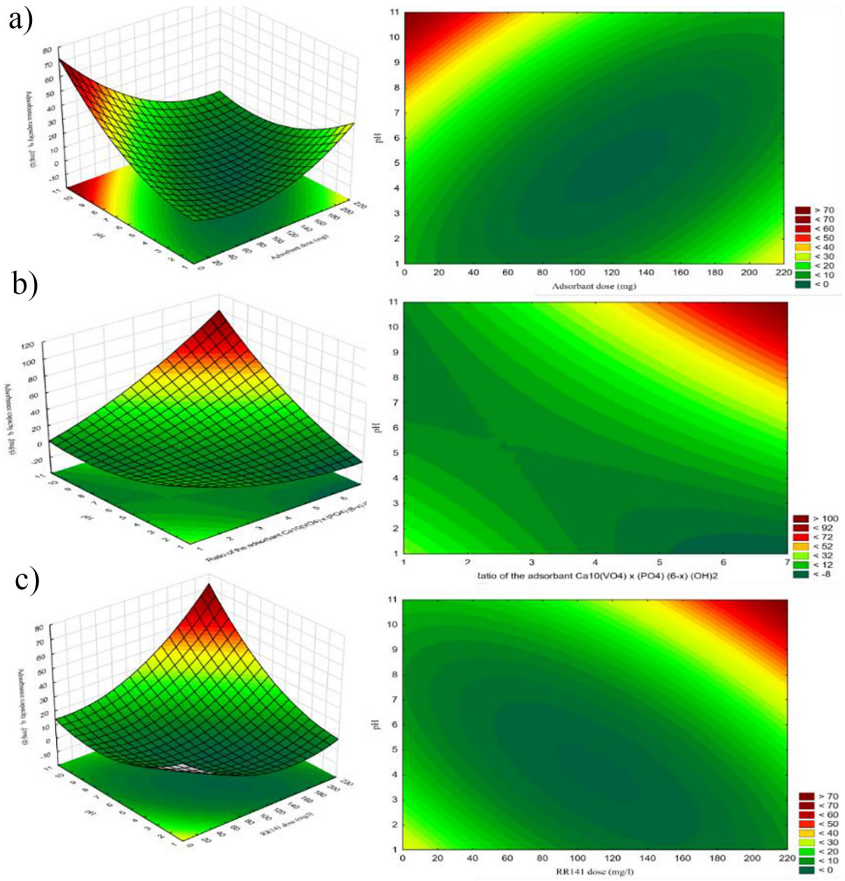

Figure 6. Contour plots and the surface response of adsorption capacity q_e ($mg \cdot g^{-1}$) according to the main effect factors: (a) pH, adsorbent dose, (b) ratio of the adsorbent, pH; (c) pH, RR141 dose

Table 9. Comparison of adsorbent performance for RR141 removal

Adsorbent	Adsorption capacity ($mg \cdot g^{-1}$)	Reference
Activated carbon	38.74	(Behloul et al. 2022)
NP/NiO	38.91	(Hafdi et al. 2020c)
Chitosan/ZIF-8	6.51	(Phonlakan et al. 2023)
$Ca_{10}(VO_4)_x(PO_4)_{6-x}(OH)_2$	50	This study

a better fit of the pseudo-second-order model to describe RR141 adsorption. these experimental studies were carried out over a range of concentrations from 5 to 150 $mg \cdot L^{-1}$ to assess the kinetics of the 4.5V-apatite adsorbent towards RR141.

Adsorption isotherme

Following the evaluation of the Freundlich, Sips, and Langmuir adsorption isotherms, the values obtained for the coefficients of determination (R^2) are 0.87, 0.80 and 0.97 respectively as shown in Table 11. Although the R^2 values for the Langmuir and Freundlich models are slightly lower, the Sips model has a high R^2 of 0.97. In comparison to the other models, these results point to a better match between the theoretical Sips model and the experimental data. The relationship between adsorbent concentrations and amounts absorbed in the system under study appears to be better represented by the Sips model. Even so The Sips model is a combination of the Langmuir and Freundlich models. This approach combines elements of both multilayer adsorption (described by the Freundlich model) and mono-molecularity (represented by the Langmuir model) in a single model. Thus, the suitability of the Sips model with a higher coefficient of determination (R^2) suggests that this model may better represent the variety of adsorption mechanisms present in the system studied, encompassing both monomolecular and multilayer layer formation on the adsorbent surface.

Using non-linear regression curves (Figure 7), several isothermal model equations (Table 3) were considered to predict how the RR141 dye will behave in relation to the adsorbent. The detailed results for the three isothermal model calculations are presented in Table 11.

Adsorption thermodynamics

Understanding thermodynamics is necessary for sorption processes. It offers details on the adsorption as well as the kind of adsorption heat. This includes entropy ($\Delta S°$), thermal adsorption ($\Delta H°$), free energy ($\Delta G°$), and the equilibrium constant K_D. The thermodynamic parameters of the adsorbents were obtained using the Langmuir adsorption isotherm constant, K_L, and the van't Hoff equation, with conventional equations Table 12.

The adsorption experiment with the RR141 dye on the adsorbent was carried out at different temperatures (308, 313, and 318 K). The adsorption capacities of adsorbents showed a linear increase when the temperature was raised from 20 to 50 °C. This observation suggests that the dye molecules have a greater propensity to interact with the adsorbent surface at higher temperatures, leading to increased adsorption capacity. Thermodynamic

Table 10. Pseudo- first -order, pseudo- second -order kinetic model for the adsorption of RR141 onto prepared adsorbent (pH = 8, adsorbent dose = 57.5 mg, ratio of the adsorbent = 4.5)

Kinetic model	Parameter	Value of the dye RR141					
		5 $mg \cdot L^{-1}$	10 $mg \cdot L^{-1}$	20 $mg \cdot L^{-1}$	50 $mg \cdot L^{-1}$	100 $mg \cdot L^{-1}$	150 $mg \cdot L^{-1}$
Pseudo first order (PSO)							
PFO	$q_{e,cal}$ ($mg \cdot g^{-1}$)	0.0699	0.9575	0.8286	2.552	18.827	15.386
	K_1 (min^{-1})	0.00156	-0.0006	0.0003	-0.0012	-0.0017	-0.0014
	R^2	0.0361	0.237	0.0628	0.3139	0.6137	0.8281
Pseudo second order (PSO)							
PSO	$q_{e,cal}$ ($mg \cdot g^{-1}$)	4.4984	4.2571	6.1728	21.598	42.1940	46.9483
	K_2 (min^{-1})	0.1137	0.2800	0.0312	0.0074	0.0024	0.0051
	R^2	0.9977	0.9909	0.9926	0.9266	0.9885	0.9966

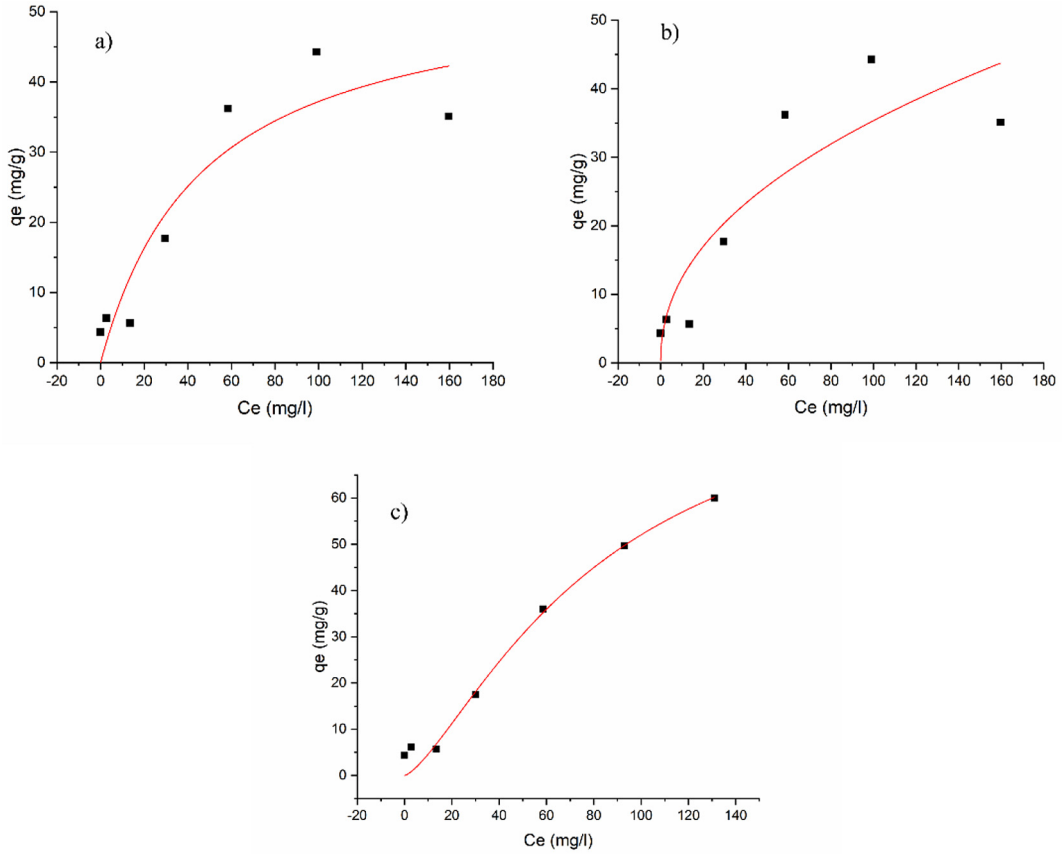

Figure 7. Adsorption isotherm of nonlinear; (a) Langmuir, (b) Freundlich, and (c) Sips

Table 11. Isotherm parameters for RR141 adsorption on the $Ca_{10}(PO_4)_{1.5}(VO_4)_{4.5}(OH)_2$

Isotherm model	Parameter	Value
Langmuir	q_{max} (mg·g^{-1})	53.7759
	K_L (mg·L^{-1})	0.02119
	R^2	**0.8701**
Freundlich	K_F mg·g^{-1} (mg·L^{-1})$^{1/n}$	4.34385
	N	2.19632
	R^2	**0.80949**
Sips	q_s	91.5059
	K_S	0.00215
	N	1.39348
	R^2	**0.98434**

parameter values are listed in Table 12. Negative values of ΔG°, at all operating temperatures, indicate spontaneous adsorption. The fact that ΔH° (-11.599 kJ·mol^{-1}) is negative, indicates that the adsorption process is exothermic. Utilizing ΔH, we can infer the adsorbent-adsorbate interactions, where physisorption is often associated with values less than 40 kJ·mol^{-1}. Positive values of ΔS° (19.0922 J·K^{-1}·mol^{-1}) signal an increase in disorder at the interface between adsorbent and adsorbate.

Adsorption mechanism

The investigation identified the point of zero charge (PZC) of $Ca_{10}(VO_4)_x(PO_4)_{6-x}(OH)_2$ at 8.73, indicating that above this pH value, the adsorbent surface becomes negatively charged, while below it, the surface carries a positive charge. As the RR141 dye is anionic, this results in an electrostatic interaction between the adsorbent and the negatively charged dye molecules. Notably, the results demonstrate that the adsorption capacity for RR141 dye reaches its maximum at pH 8, with a capacity of 50 mg·g^{-1}.

CONCLUSIONS

We conclude that this study highlights the critical need for developing a novel adsorbent for the removal of the RR141 dye using NPs-HAP-VAP adsorbents derived from solid waste. The results reveal a coefficient of determination (R^2) of 0.995, confirming the robustness and accuracy of the adsorption model developed using the CCD. The optimal conditions determined, including a specific incorporation ratio of 4.5, adsorbent dose of

Table 12. Formulas and thermodynamic parameter for RR141 adsorption on the $Ca_{10}(PO_4)_{1.5}(VO_4)_{4.5}(OH)_2$

Equation (y = 1395.2x+ 2.2964 R² = 0.9782)	*T* (K)	K_L (mg·L^{-1})	LnK_d	Δ*G*° (kJ·mol^{-1})	Δ*H*° (kJ·mol^{-1})	Δ*S*° (J·K^{-1}·mol^{-1})
Van't hoff equation: $LnK_L = 1/K_d+1/T$ $K_L = q_e/C_e$ $\Delta G° = -R·T·LnK_d$ $\Delta G° = \Delta H°–T.\Delta S°$	293.15	1132.293801	20.8475	-50.810	-11.5996	19.0922
	303.15	1032.698825	20.7554	-52.311		
	313.15	847.5982817	20.5579	-53.523		
	323.15	739.2219038	20.4211	-54.864		

57.5 mg, dye concentration of 157.5 mg·L^{-1}, pH of 8, and contact time of 92.5 min, played a crucial role in achieving maximum removal capacity of the RR141 dye. This study demonstrated an adsorption capacity of 50 mg·g^{-1}, with a percentage removal reaching 100%. The RR-141 removal follows the pseudo-second order and the SIPS model. Thermodynamic calculations showed spontaneous adsorption, suggesting that the physical character is enhanced by positive entropy variations. These findings demonstrate the remarkable effectiveness of this approach to pollution control, which offers hopeful prospects for sustainable waste management and environmental protection.

Acknowledgments

The authors would like to greatly acknowledge the financial support of funding from the University of Chouaib Doukkali, El Jadida, Morocco.

REFERENCES

1. Aguareles, M., Barrabés, E., Myers, T., Valverde, A. 2023. Mathematical analysis of a Sips-based model for column adsorption. Physica D: Nonlinear Phenomena, 448, 133690. https://doi.org/10.1016/j.physd.2023.133690
2. Ahmed, J., Thakur, A., Goyal, A. 2021. Industrial wastewater and its toxic effects. https://pubs.rsc.org/en/content/chapterhtml/2021/bk9781839162794-00001?isbn=978-1-83916-279-4&sercode=bk. Accessed 12 November 2023
3. Ajiboye, T. O., Oyewo, O.A., Onwudiwe, D.C. 2021. Simultaneous removal of organics and heavy metals from industrial wastewater: A review. Chemosphere, 262, 128379.
4. Alabdraba, W., Bayati, M. 2014. Biodegradation of Azo dyes a review. Int. J. Environ. Eng. Nat. Resour, 1(4), 179–189.
5. Anastopoulos, I., Kyzas, G.Z. 2014. Agricultural peels for dye adsorption: a review of recent literature. Journal of Molecular Liquids, 200, 381–389.
6. Bafana, A., Devi, S.S., Chakrabarti, T. 2011. Azo dyes: past, present and the future. Environmental Reviews, 19(NA), 350–371. https://doi.org/10.1139/a11-018
7. Behloul, H., Ferkous, H., Bougdah, N., Djellali, S., Alam, M., Djilani, C., Sedik A., Lerari D., Jeon B.-H., Benguerba Y. 2022. New insights on the adsorption of CI-Reactive Red 141 dye using activated carbon prepared from the ZnCl2-treated waste cotton fibers: Statistical physics, DFT, COSMO-RS, and AIM studies. Journal of Molecular Liquids, 364, 119956. https://doi.org/10.1016/j.molliq.2022.119956
8. Bezerra, M.A., Santelli, R.E., Oliveira, E.P., Villar, L.S., Escaleira, L.A. 2008. Response surface methodology (RSM) as a tool for optimization in analytical chemistry. Talanta, 76(5), 965–977. https://doi.org/10.1016/j.talanta.2008.05.019
9. Bonyadi, Z., Fouladi, Z., Robatjazi, A., Zahmatkesh Anbarani, M. 2022. Reactive red-141 removal from synthetic solutions by γ-Al_2O_3 nanoparticles: process modeling, kinetic, and isotherm studies. Applied Water Science, 13(2), 52. https://doi.org/10.1007/s13201-022-01854-6
10. Bouchelkia, N., Tahraoui, H., Amrane, A., Belkacemi, H., Bollinger, J.-C., Bouzaza, A., Abdelhalim Zoukel, Jie Zhang, Lotfi Mouni. 2023. Jujube stones based highly efficient activated carbon for methylene blue adsorption: Kinetics and isotherms modeling, thermodynamics and mechanism study, optimization via response surface methodology and machine learning approaches. Process Safety and Environmental Protection, 170, 513–535. https://doi.org/10.1016/j.psep.2022.12.028
11. Chajri, F.Z., Bensemlali, M., Nasrellah, H., Hatimi, B., Aarfane, A., Monkade, M. 2024. A New One-Step Synthesis of Nanostructured Calcium Vanadate/Phosphate Apatite for Vanadate and Phosphorus Waste Valorisation: Characterization and Band Gap Determination. Biointerface Research in Applied Chemistry, 14(2). https://doi.org/10.33263/BRIAC142.040
12. Chung, K.-T. 2016. Azo dyes and human health: A review. Journal of Environmental Science and Health, Part C, 34(4), 233–261. https://doi.org/10.1080/10590501.2016.1236602
13. Driouich, A., Chajri, F., El Hassani, S.E.A., Britel,

O., Belouafa, S., Khabbazi, A., Chaair, H. 2020. Optimization synthesis geopolymer based mixture metakaolin and fly ash activated by alkaline solution. Journal of Non-Crystalline Solids, 544, 120197.

14. Eltaboni, F., Bader, N., El-Kailany, R., Elsharif, N., Ahmida, A. 2022. Dyes: a comprehensive review. J. Chem. Rev., 2022, 4.
15. Esbensen, K. H., Guyot, D., Westad, F., Houmoller, L. P. 2002. Multivariate data analysis: in practice: an introduction to multivariate data analysis and experimental design. Multivariate Data Analysis.
16. Ezzati, R. 2020. Derivation of pseudo-first-order, pseudo-second-order and modified pseudo-first-order rate equations from Langmuir and Freundlich isotherms for adsorption. Chemical Engineering Journal, 392, 123705.
17. Ganta, D. D., Hirpaye, B. Y., Raghavanpillai, S. K., Menber, S. Y. 2022. Green synthesis of hydroxyapatite nanoparticles using Monoon longifolium leaf extract for removal of fluoride from aqueous solution. Journal of Chemistry, 2022. https://www.hindawi.com/journals/jchem/2022/4917604/. Accessed 14 November 2023
18. Garg, S. K., Tripathi, M. 2017. Microbial strategies for discoloration and detoxification of azo dyes from textile effluents. Research Journal of Microbiology, 12(1), 1–19.
19. Hafdi, H., Joudi, M., Mouldar, J., Hatimi, B., Nasrellah, H., El Mhammedi, M. A., Bakasse, M. 2020a. Design of a new low cost natural phosphate doped by nickel oxide nanoparticles for capacitive adsorption of reactive red 141 azo dye. Environmental research, 184, 109322.
20. Hafdi, H., Joudi, M., Mouldar, J., Hatimi, B., Nasrellah, H., El Mhammedi, M. A., Bakasse, M. 2020b. Design of a new low cost natural phosphate doped by nickel oxide nanoparticles for capacitive adsorption of reactive red 141 azo dye. Environmental Research, 184, 109322. https://doi.org/10.1016/j.envres.2020.109322
21. Hafdi, H., Joudi, M., Mouldar, J., Hatimi, B., Nasrellah, H., El Mhammedi, M. A., Bakasse, M. 2020c. Design of a new low cost natural phosphate doped by nickel oxide nanoparticles for capacitive adsorption of reactive red 141 azo dye. Environmental Research, 184, 109322. https://doi.org/10.1016/j.envres.2020.109322
22. Hashemi, S. H., Kaykhaii, M. 2022. Azo dyes: sources, occurrence, toxicity, sampling, analysis, and their removal methods. In Emerging freshwater pollutants 267–287. Elsevier. https://www.sciencedirect.com/science/article/pii/B9780128228500000132. Accessed 12 November 2023
23. Hilbe, J. M. 2007. STATISTICA 7: An Overview. The American Statistician, 61(1), 91–94. https://doi.org/10.1198/000313007X172998
24. Holkar, C. R., Jadhav, A. J., Pinjari, D. V., Mahamuni, N. M., Pandit, A. B. 2016. A critical review on textile wastewater treatments: Possible approaches. Journal of Environmental Management, 182, 351–366. https://doi.org/10.1016/j.jenvman.2016.07.090
25. Ibitoye, F. O., Imarhiagbe, E. E., Ekhaise, F. O. 2022. A review on the ecological impacts of azo dye and survey of bioremediation potential strains. Journal of Science and Technology Research, 4(3). https://journals.nipes.org/index.php/njstr/article/download/374/391. Accessed 12 November 2023
26. Ibrahim, M., Labaki, M., Giraudon, J.-M., Lamonier, J.-F. 2020. Hydroxyapatite, a multifunctional material for air, water and soil pollution control: A review. Journal of hazardous materials, 383, 121139.
27. Jaafar, A., Darchen, A., Hamzi, S. E., Lakbaibi, Z., Driouich, A., Boussaoud, A., Abdelrani Yaacoubi, Mohammed El Makhfouk, Mohsine Hachkar. 2021. Optimization of cadmium ions biosorption by fish scale from aqueous solutions using factorial design analysis and Monte Carlo simulation studies. Journal of Environmental Chemical Engineering, 9(1), 104727. https://doi.org/10.1016/j.jece.2020.104727
28. Jebli, A., Amri, A. E., Hsissou, R., Lebkiri, A., Zarrik, B., Bouhassane, F. Z., Hbaiz El M., Rifi El H., Lebkiri A. 2023. Synthesis of a chitosan@hydroxyapatite composite hybrid using a new approach for high-performance removal of crystal violet dye in aqueous solution, equilibrium isotherms and process optimization. Journal of the Taiwan Institute of Chemical Engineers, 149, 105006. https://doi.org/10.1016/j.jtice.2023.105006
29. JMP. 2023. JMP Pro, version 16. SAS Institute Inc Cary (NC).
30. Jokić Govedarica, J., Tomašević Pilipović, D., Gvoić, V., Kerkez, Đ., Leovac Maćerak, A., Slijepčević, N., Bečelić-Tomin, M. 2024. Eco-friendly nanoparticles: mechanisms and capacities for efficient removal of heavy metals and phosphate from water using definitive screening design approach. Environmental Geochemistry and Health, 46(4), 118. https://doi.org/10.1007/s10653-024-01879-7
31. Jones, B., Sall, J. 2011. JMP statistical discovery software. WIREs Computational Statistics, 3(3), 188–194. https://doi.org/10.1002/wics.162
32. Joudi, M., Nasserlah, H., Hafdi, H., Mouldar, J., Hatimi, B., Mhammedi, M. A. E., Bakasse, M. 2020. Synthesis of an efficient hydroxyapatite–chitosan–montmorillonite thin film for the adsorption of anionic and cationic dyes: adsorption isotherm, kinetic and thermodynamic study. SN Applied Sciences, 2(6), 1078. https://doi.org/10.1007/s42452-020-2848-3
33. Khan, R., Bhawana, P., Fulekar, M. H. 2013. Microbial decolorization and degradation of synthetic dyes: a review. Reviews in Environmental Science and Bio/Technology, 12(1), 75–97. https://doi.

org/10.1007/s11157-012-9287-6

34. Kosmulski, M. 2014. The pH dependent surface charging and points of zero charge. VI. Update. Journal of Colloid and Interface Science, 426, 209–212. https://doi.org/10.1016/j.jcis.2014.02.036
35. Liang, L., Wang, Z., Li, J. 2019. The effect of urbanization on environmental pollution in rapidly developing urban agglomerations. Journal of cleaner production, 237, 117649.
36. Lin, L., Yang, H., Xu, X. 2022. Effects of water pollution on human health and disease heterogeneity: a review. Frontiers in environmental science, 10, 880246.
37. Liu, Q. 2020. Pollution and treatment of dye waste-water. In: IOP Conference Series: Earth and Environmental Science 514, 052001). IOP Publishing. https://iopscience.iop.org/article/10.1088/1755-1315/514/5/052001/meta. Accessed 12 November 2023
38. Morin-Crini, N., Lichtfouse, E., Liu, G., Balaram, V., Ribeiro, A.R.L., Lu, Z., Stock, F., Carmona, E., Teixeira, M.R., Picos-Corrales, L.A., Moreno-Piraján, J.A., Giraldo, L. Li, C., Pandey, A., Hocquet, D., Torri, G., Crini, G. 2022. Worldwide cases of water pollution by emerging contaminants: a review. Environmental Chemistry Letters, 20(4), 2311–2338. https://doi.org/10.1007/s10311-022-01447-4
39. Pai, S., Kini, M.S., Selvaraj, R. 2021. A review on adsorptive removal of dyes from wastewater by hydroxyapatite nanocomposites. Environmental Science and Pollution Research, 28(10), 11835–11849. https://doi.org/10.1007/s11356-019-07319-9
40. Phonlakan, K., Khamsuk, B., Soontonhong, N., Panawong, C., Kongseng, P., Chantarak, S., Budsombat, S. 2023. Composite beads from chitosan and zeolitic imidazolate framework-8 for the adsorption and photocatalytic degradation of reactive red 141. RSC Advances, 13(18), 12295–12308. https://doi.org/10.1039/D3RA01187A
41. Revellame, E.D., Fortela, D.L., Sharp, W., Hernandez, R., Zappi, M. E. 2020. Adsorption kinetic modeling using pseudo-first order and pseudo-second order rate laws: A review. Cleaner Engineering and Technology, 1, 100032.
42. Rodrigues, E., Almeida, O., Brasil, H., Moraes, D., dos Reis, M.A.L. 2019. Adsorption of chromium (VI) on hydrotalcite-hydroxyapatite material doped with carbon nanotubes: Equilibrium, kinetic and thermodynamic study. Applied Clay Science, 172, 57–64. https://doi.org/10.1016/j.clay.2019.02.018
43. Sansenya, T., Masri, N., Chankhanittha, T., Senasu, T., Piriyanon, J., Mukdasai, S., Nanan, S. 2022. Hydrothermal synthesis of ZnO photocatalyst for detoxification of anionic azo dyes and antibiotic. Journal of Physics and Chemistry of Solids, 160, 110353. https://doi.org/10.1016/j.jpcs.2021.110353
44. Saratale, R.G., Saratale, G.D., Chang, J.-S., Govindwar, S.P. 2011. Bacterial decolorization and degradation of azo dyes: a review. Journal of the Taiwan institute of Chemical Engineers, 42(1), 138–157.
45. Sharma, J., Sharma, S., Soni, V. 2021. Classification and impact of synthetic textile dyes on Aquatic Flora: A review. Regional Studies in Marine Science, 45, 101802.
46. Singh, N., Poonia, T., Siwal, S.S., Srivastav, A. L., Sharma, H.K., Mittal, S.K. 2022. Challenges of water contamination in urban areas. In Current directions in water scarcity research 6, 173–202. Elsevier. https://www.sciencedirect.com/science/article/pii/B9780323918381000087. Accessed 12 November 2023
47. Sophia A.C., Lima, E.C. 2018. Removal of emerging contaminants from the environment by adsorption. Ecotoxicology and Environmental Safety, 150, 1–17. https://doi.org/10.1016/j.ecoenv.2017.12.026
48. Srikaew, M., Jumpapaeng, P., Suwanakood, P., Kaiyasuan, C., Promarak, V., Saengsuwan, S. 2023. Rapid synthesis and optimization of UV-photopolymerized cassava starch-based superabsorbent hydrogels as a biodegradable, low-cost, and effective adsorbent for MB removal. Journal of Industrial and Engineering Chemistry, 118, 53–69. https://doi.org/10.1016/j.jiec.2022.10.045
49. Statsoft, I.N.C. 2013. STATISTICA (data analysis software system), ver. 12. Tulsa, OK, USA.
50. Willmott, C.J. 1981. On the validation of models. Physical Geography. https://www.tandfonline.com/doi/abs/10.1080/02723646.1981.10642213. Accessed 26 September 2023